IOP Publishing Nanotechnology
Nanotechnology 26 (2015) 275604 (8pp) doi:10.1088/0957-4484/26/27/275604

Construction and characterization of Cu^{2+}, Ni^{2+}, Zn^{2+}, and Co^{2+} modified-DNA crystals

Sreekantha Reddy Dugasani[1,2], Myoungsoon Kim[3], In-yeal Lee[2,4], Jang Ah Kim[2,5], Bramaramba Gnapareddy[1,2], Keun Woo Lee[1], Taesung Kim[2,5], Nam Huh[3], Gil-Ho Kim[2,4], Sang Chul Park[3] and Sung Ha Park[1,2]

[1] Department of Physics, Sungkyunkwan University, Suwon 440-746, Korea
[2] Sungkyunkwan Advanced Institute of Nanotechnology (SAINT), Sungkyunkwan University, Suwon 440-746, Korea
[3] Well Aging Research Center, Samsung Advanced Institute of Technology (SAIT), Suwon 443 803, Korea
[4] School of Electronic and Electrical Engineering, Sungkyunkwan University, Suwon 440-746, Korea
[5] Department of Mechanical Engineering, Sungkyunkwan University, Suwon 440-746, Korea

E-mail: ghkim@skku.edu, sc2013.park@samsung.com and sunghapark@skku.edu

Received 25 February 2015, revised 15 May 2015
Accepted for publication 19 May 2015
Published 18 June 2015

Abstract

We studied the physical characteristics of modified-DNA (M-DNA) double crossover crystals fabricated via substrate-assisted growth with various concentrations of four different divalent metallic ions, Cu^{2+}, Ni^{2+}, Zn^{2+}, and Co^{2+}. Atomic force microscopy (AFM) was used to test the stability of the M-DNA crystals with different metal ion concentrations. The AFM images show that M-DNA crystals formed without deformation at up to the critical concentrations of 6 mM of [Cu^{2+}], 1.5 mM of [Ni^{2+}], 1 mM of [Zn^{2+}], and 1 mM of [Co^{2+}]. Above these critical concentrations, the M-DNA crystals exhibited deformed, amorphous structures. Raman spectroscopy was then used to identify the preference of the metal ion coordinate sites. The intensities of the Raman bands gradually decreased as the concentration of the metal ions increased, and when the metal ion concentrations increased beyond the critical values, the Raman band of the amorphous M-DNA was significantly suppressed. The metal ions had a preferential binding order in the DNA molecules with G–C and A–T base pairs followed by the phosphate backbone. A two-probe station was used to measure the electrical current–voltage properties of the crystals which indicated that the maximum currents of the M-DNA complexes could be achieved at around the critical concentration of each ion. We expect that the functionalized ion-doped M-DNA crystals will allow for efficient devices and sensors to be fabricated in the near future.

S Online supplementary data available from stacks.iop.org/NANO/26/275604/mmedia

Keywords: DNA self-assembly, metal ion, modified-DNA, Raman, electrical characteristics

(Some figures may appear in colour only in the online journal)

1. Introduction

Recent breakthroughs in DNA nanotechnology have indicated that artificial DNA nanostructures, rather than single strand or duplex modified-DNA (M-DNA), will have extensive applicability in a variety of fields, such as for spintronics [1, 2], nanoelectronics [3, 4], biosensors [5, 6] and nanophotonics [7]. DNA is a particularly promising source of self-organizing material, and it serves as a useful building block for bionanotechnology [8]. The exceptional programmability of DNA, i.e., the ability to design and program a DNA base sequence, allows for highly selective binding that creates complex DNA nanostructures in one-, two-, and three-(1D-, 2D-, and 3D-) dimensions [9–14]. Structural DNA

nanotechnology involves researchers from the physical and biological sciences who come together and engage in interesting multidisciplinary research [14–16]. The DNA nanostructures can be easily conjugated with other nanomaterials, such as proteins [16], nanoparticles [17, 18], or nanowires [19, 20] by using a simple molecular modification. Additionally, various metal ions can be incorporated into DNA to allow for the functionality to be transferred [21, 22] which makes DNA molecules good candidates for use as functionalized biomaterials for applications in traditional science and engineering.

However, the selective incorporation of metal into the DNA molecules should be considered according to the target application because different metal ions have different properties, like a good conductivity (Cu^{2+}) or a ferromagnetic nature (Ni^{2+}, Co^{2+}). A few studies have shown the functionality of analytes in the form of single and duplex M-DNA, but artificially designed periodic DNA crystals grown on a substrate have not been sufficiently studied. If the properties of M-DNA nanostructures artificially grown on a given substrate were to be determined, research would be facilitated for applications such as bioelectronics, biophotonics, biomedicine, and spintronics. Since DNA molecules allow for a high degree of customization for the geometries, scientists have suggested the possibility of using DNA molecules as electronic circuits without having to design any new circuits. However, the physical characteristics of DNA, especially for use in electronics, are yet to be clearly described, and consequently, many articles have reported that these exhibit different characteristics depending on the environment, including acting as an insulator [23], semiconductor [24, 25], conductor [26], or even a superconductor [27]. Most researchers have found DNA to be a poor conductor, at least at room temperature, so its conductivity should be improved in order to allow functional electronic devices and sensors to be constructed. In this study, we report on the fabrication of various metal ion-coordinated double-crossover (DX) tile-based DNA crystals that were grown on a glass substrate via surface assisted growth (SAG). In order to verify a consistent crystal formation and modification of the metal ions into the DNA, we investigated the atomic force microscopy (AFM) images, Raman spectra and current–voltage (*I–V*) characteristics of the fabricated M-DNA crystals.

2. Experimental section

2.1. Pretreatment of glass substrate

A $5 \times 5\,mm^2$ glass substrate was cleaned for 30 min in a piranha solution (1:2 ratio of H_2O_2 : H_2SO_4), followed by rinsing with de-ionized (DI) water. The clean substrates were then immersed into a petri-dish filled with DI water for a few hours before use.

2.2. DNA crystal growth on the glass

Due to the piranha treatment, the glass surface was functionalized with hydroxyl (-OH) groups to change its behavior from hydrophobic to hydrophilic. This allows for the DNA to bind to the substrate during the growth process. Synthetic oligonucleotides purified via high-performance liquid chromatography were purchased from BIONEER (Daejeon, Korea) and complexes containing an equimolar mixture of 8 different DX strands were formed by mixing with physiological 1× TAE/Mg^{2+} buffer solution (40 mM Tris base, 20 mM Acetic acid, 1 mM EDTA (pH 8.0), and 12.5 mM magnesium acetate). For annealing, the substrates and the DNA strands were inserted into an AXYGEN-tube with a total sample volume of 250 μL and were then placed in a Styrofoam box with 2 L of boiled water to cool slowly from 95 °C to 25 °C over a period of at least 24 h in order to facilitate hybridization. During annealing, the DX strands form polycrystalline DX lattices on the substrate, and consequently, this structure completely covers the surface of the glass. We prepared a sample with a DX concentration of 70 nM, which is well above the saturation concentration of 20 nM, to provide full coverage of the DX crystals on surface of the substrate.

2.3. Metal ion coordination

Before annealing method: metal ion modification was carried out with 250 μL of 70 nM DX strands mixed with the appropriate concentrations of copper ion solution [$Cu(NO_3)_2$] (6, 8, and 10 mM), nickel ion solution [$NiCl_2$] (1, 1.5, 2, and 4 mM), zinc ion solution [$ZnCl_2$] (0.6, 1, 2, and 4 mM), and cobalt ion solution [$CoCl_2$] (0.6, 1, 1.5, and 4 mM) before inserting the substrate into the given test tube (figure 1(a)). *After annealing method*: the appropriate amount of 1 M concentration of each metal ion was added to the DX crystals on the glass substrate, which were then incubated at room temperature for 24 h (figure 3(a)).

2.4. AFM imaging

For AFM imaging, the SAG DNA sample was placed on a metal puck using instant glue. 20 μL of 1× TAE/Mg^{2+} buffer was then pippetted onto the sample substrate and another 10 μL of 1× TAE/Mg^{2+} buffer was dispensed on a silicon nitride AFM tip (Veeco, USA). The AFM images were obtained by using a Multimode Nanoscope (Veeco, USA) in the liquid tapping mode.

2.5. Raman measurement

Before obtaining the Raman spectra, all of the samples were rinsed with DI water followed by fine blowing with nitrogen gas to remove chemical residues from the surface of the M-DNA crystals. In order to avoid optical loss due to transmission through the transparent glass, the M-DNA samples were placed on a metal puck using instant glue. The measurements were then performed at room temperature with a confocal Raman microscope (WITEC, alpha 300R) at 532 nm. The spectral reading was obtained with a 600 gr mm^{-1} diffraction grating and a height for each blade of 500 nm.

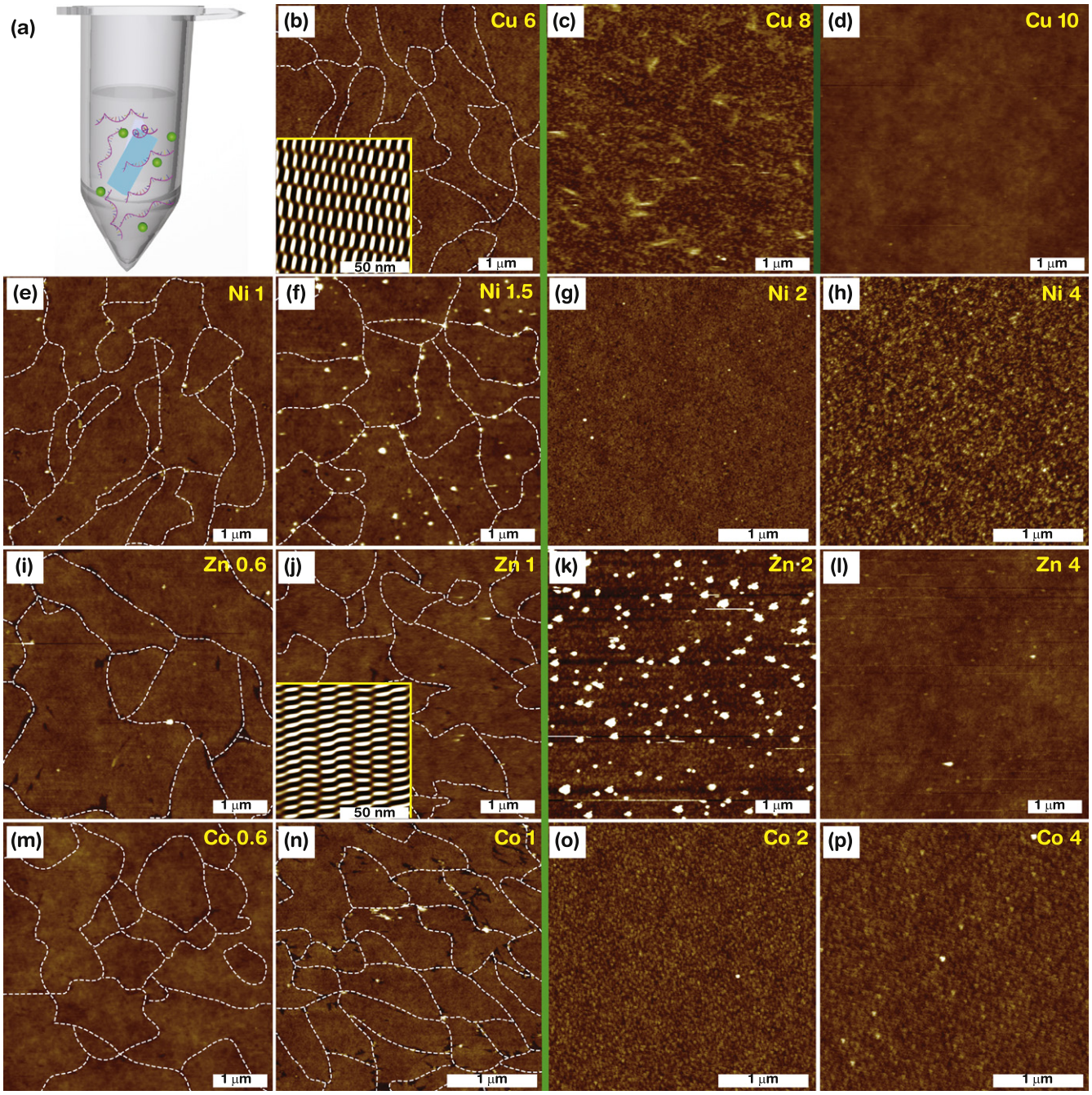

Figure 1. A cartoon of the metal ion added before annealing and the AFM images of the M-DNA double-crossover crystals coordinated with four different divalent metal ions. The white dotted lines in the images indicate the crystal domain boundaries. (a) Schematic diagram of metal ions (indicated as small green spheres) added before annealing; (b)–(d) M-DNA with 6, 8 and 10 mM of [Cu^{2+}] labeled as Cu 6, Cu 8, and Cu 10, respectively. The inset image in (b) shows the Fourier transform-mode. (e)–(h) M-DNA with 1, 1.5, 2, and 4 mM of [Ni^{2+}]. (i)–(l) M-DNA with 0.6, 1, 2, and 4 mM of [Zn^{2+}]. The inset in (j) shows the Fourier transform-mode. (m)–(p) M-DNA with 0.6, 1, 2, and 4 mM of [Co^{2+}]. On the left-hand side of the light green line, crystals without deformation for each metal ion into DNA were formed. This means that the DNA crystals were well formed at up to 6 mM of [Cu^{2+}], 1.5 mM of [Ni^{2+}], 1 mM of [Zn^{2+}], and [Co^{2+}] into DNA. Above these concentrations, the M-DNA DX crystal structures appeared aggregated and amorphous. 8 mM of [Cu^{2+}] into DNA (between the light and dark green lines, (c)) showed small DX lattice fragments along with aggregated ones.

2.6. Electrical measurements

The M-DNA samples were cleaned with DI water and were then softly dried with nitrogen gas to remove residual water from the M-DNA surface. Then, silver paste was deposited on the M-DNA surface to create a metal contact, and the channel gap was fixed at approximately 1 mm. The *I–V* characteristics of M-DNA crystals were measured using a Keithely Electrical Measurement Unit (SCS-4200). A schematic diagram of the simple two-terminal (source and drain) probe station for the

electrical characteristic measurement of M-DNA samples was shown in figure S1 (available at stacks.iop.org/NANO/26/275604/mmedia).

3. Results and discussion

We initially obtained the Raman spectra on the mica substrate. Mica is commonly used in biological imaging with AFM due to its intrinsic net charge and atomically flat nature. The Raman band positions of mica and of DNA on mica are similar to each other because mica consists of minerals with other metal impurities. Consequently it is difficult to estimate the Raman bands for the M-DNA complex when mica is used. In order to eliminate the undesirable effects of using a mica substrate, we introduced a glass substrate to perform an adequate Raman analysis. The Raman spectra of glass, mica, and DNA on mica are shown in figure S2 (online supplementary data).

Four different divalent metal ions, Cu^{2+}, Ni^{2+}, Zn^{2+} and Co^{2+} coordinated on DX polycrystalline DNA structures at various concentrations were formed on glass via SAG. Two DX tiles (DX-1 and DX-2, see online supplementary data figure S3 and tables S1, S2 for details) were used to construct 2D DNA crystal structures on the given substrate (The detailed sample preparation was discussed in the experimental section). First, the experimental procedure was adopted by adding metal ions into the DNA buffer solution before annealing in order to verify the stability of the DNA crystals with ions and the structural phase transitions during annealing. The experimental schematic for the metal ions added before annealing is shown in figure 1(a). For consistency during annealing, the thermal energy was controlled during an annealing time of 24 h while the electrostatic interaction between the substrate with a size of $5 \times 5\ mm^2$ and the DNA molecules and the total sample volume of 250 μL in the test tube were fixed. The concentrations of the metal ions were then used as control parameters.

Figure 1 shows the AFM images of the M-DNA with varying concentrations of metal ions. The white dotted line in the images indicates the 2D DNA crystal boundaries. In the images, copper ion [Cu^{2+}] of 6, 8, and 10 mM in the DNA structures are marked as Cu 6, Cu 8, and Cu 10; nickel ion [Ni^{2+}] of 1, 1.5, 2, and 4 mM are marked as Ni 1, Ni 1.5, Ni 2, and Ni 4; zinc ion [Zn^{2+}] of 0.6, 1, 2, and 4 mM are marked as Zn 0.6, Zn 1, Zn 2, and Zn 4; and cobalt ion [Co^{2+}] of 0.6, 1, 2, and 4 mM are marked as Co 0.6, Co 1, Co 2, and Co 4, respectively. The insets in the bottom left in figures 1(b), (j) were the noise-filtered 2D spectrum images according to fast Fourier transform showing the periodicity of the unit building block (DX tile). Figure 1 shows the structural phase transitions according to changes in the concentrations of the metal ions. A vertical light-green line separates the crystalline and aggregate/amorphous phases. The left side of this line shows the approximate saturation concentration (C_s) of each metal ion for which the DNA crystals were not deformed, which means that the surface morphology of the M-DNA crystals is stable at up to 6 mM of [Cu^{2+}], 1.5 mM of [Ni^{2+}], 1 mM of [Zn^{2+}], and [Co^{2+}]. Beyond these levels, all of the M-DNA complexes exhibited aggregated and/or amorphous structures. Interestingly, the 8 mM [Cu^{2+}], shown in figure 1(c), that is located between the light and dark green lines shows small crystal fragment along with aggregated structures while the 10 mM [Cu^{2+}] shows amorphous structures without domain boundaries and crystal periodicity. Generally these phase regions can be considered to be a crystal stability region ($\leqslant C_s$) and a structural denaturing region ($>C_s$) due to the presence of ions. The crystal stability region is important because the functionality embedded into the crystalline DNA structures can play a role in the fabrication of nano-scale devices and sensors. F Moreno-Herrero *et al* [28] had discussed the topographic characteristics and the electrostatic response of duplex M-DNA, and we also noticed that the M-DNA crystals with C_s exhibit extreme magnetic characteristics relative to crystals with other concentrations [29].

The helical structure of DNA molecules is heavily dependent upon the composition of the buffer solution, pH, and humidity as well as the concentration of metal ions. The denaturing phenomenon depends on whether the pH is lower or higher than 8 when the ions are added before annealing. Since the DNA molecules are dissolved in a common 1× TAE/Mg^{2+} buffer with the metal ion solution, they are unstable during hybridization if we increase the concentration of metal ions higher than C_s into the test tube before annealing. Therefore a higher entropic cost is incurred in order to form M-DNA polycrystalline structures without denaturing on the substrate. The structural M-DNA phase transitions can be explained according to the substitutional and interstitial bindings, and at a low concentration of metal ions into the DNA, the substitutional bindings are dominated. However, at a higher concentration, the interstitial bindings also play a role. In the substitutional case, the crystal structure is minimally deformed because the metal ions are systematically coordinated with particular sites. In the interstitial case, the structure may be more severely damaged and deformed because the metal ions are randomly coordinated within the DNA duplex.

The crystal stability and the structural phase transitions were also verified by measuring the Raman band intensities via Raman spectroscopy. The structure of the M-DNA with the metal ion bindings can be indirectly verified via chemical reduction and current measurements [30]. In contrast, the Raman spectroscopy allows for direct measurement to understand the binding sites between the metal ions and DNA molecules and also reveals the details of the binding mechanism. A few studies have partially investigated analytes in the form of single and duplex M-DNA with specific metal ion bindings [31–33]. Figure 2 shows the Raman spectra for various metal ion concentrations in the M-DNA structures and the resulting analysis. The DNA crystals without metal ions show vibration/stretching Raman modes/bands centered around 1246 and 1420 cm^{-1} for adenine (A); 770 and 1469 cm^{-1} for thymine (T); 931 and 1590 cm^{-1} for guanine (G); 618, 655, and 1348 cm^{-1} for cytosine (C); and 1066 and 1145 cm^{-1} for the phosphate backbone $\left(PO_4^-\right)$ [31–35].

The Raman spectra of M-DNA complexes were generated in order to trace the intensity variations in the Raman bands resulting from the interaction with the ions. An increase

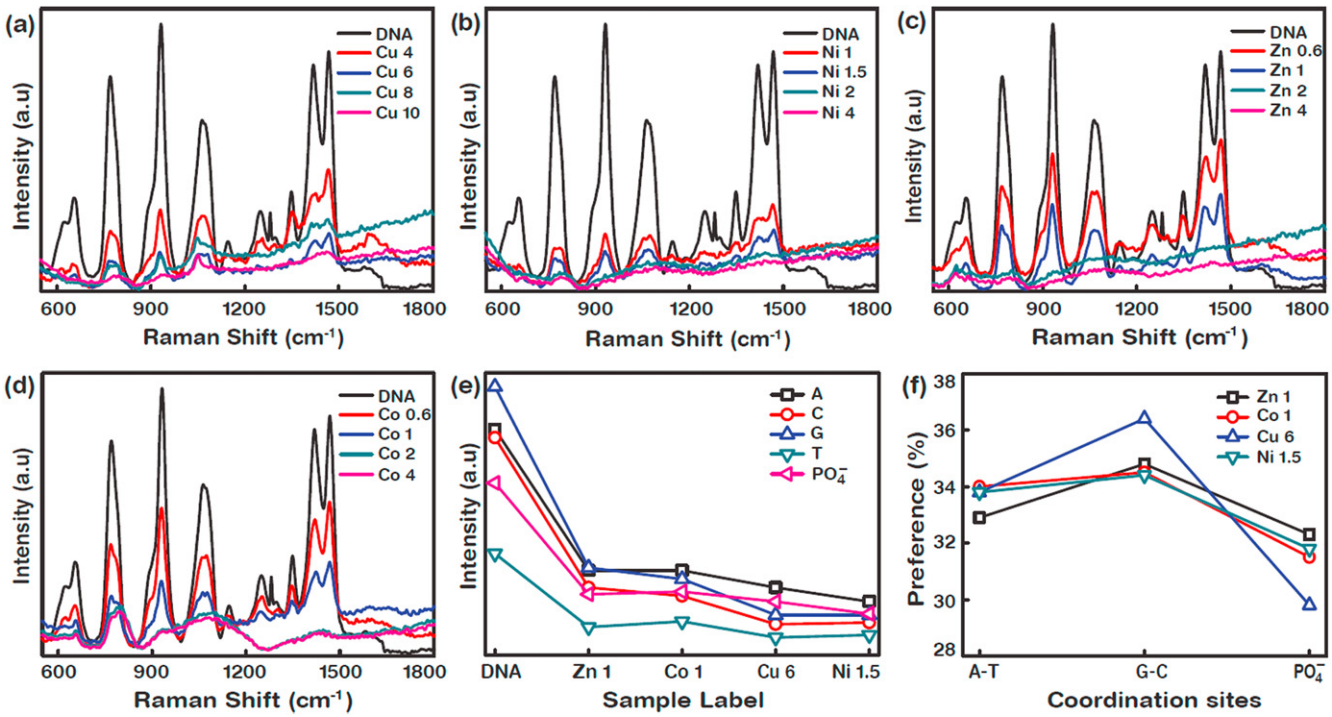

Figure 2. Analysis of the Raman spectra for M-DNA complexes before and after structural denaturing with various concentrations of metal ions into DNA. The Raman spectra for various concentrations of (a) Cu^{2+}-DNA complexes, (b) Ni^{2+}-DNA, (c) Zn^{2+}-DNA, and (d) Co^{2+}-DNA. (e) The variation in intensity for adenine (A), cytosine (C), guanine (G), thymine (T), and the phosphate backbone (PO_4^-) of the DNA and M-DNA crystals at a saturation concentration C_s of each metal ion: Zn 1, Co 1, Cu 6, and Ni 1.5. (f) Preferences of the metal ion coordinate sites in DNA at C_s for each metal ion.

in the [Cu^{2+}] into DNA (figure 2(a)) results in a considerable decrease in the intensity of all vibrational and stretching bands throughout the spectrum. At 8 and 10 mM of [Cu^{2+}], only a few bands are observed that correspond with T, G, PO_4^-, A, T at 770, 931, 1061, 1420, and 1469 cm^{-1}, respectively. With an increase of up to 1.5 mM of [Ni^{2+}] into the DNA (figure 2(b)), the vibration bands gradually decrease, and after 1.5 mM of [Ni^{2+}] only the vibrational Raman bands of T, PO_4^-, and A at 770, 1066, and 1430 cm^{-1} were observed. With an increase of up to 1 mM of [Zn^{2+}] and [Co^{2+}] into the DNA (figures 2(c) and (d)) a considerable decrease in the intensity can be observed throughout the spectrum. After 1 mM of [Zn^{2+}] and [Co^{2+}] into DNA, only the vibration Raman bands of C, T and PO_4^- at 618, 770, and 1066 cm^{-1} were observed, and all other bands were suppressed. All M-DNA complexes at higher metal ion concentrations (higher than C_s) exhibit a few of bands that were slightly shifted, and all band intensities decreased as the concentration increased.

Figure 2(e) shows the variation in the intensity of A, C, G, T, and PO_4^- sites of the DNA and M-DNA with C_s of the four metal ions at 1 mM for [Zn^{2+}] and [Co^{2+}], 6 mM for [Cu^{2+}], and 1.5 mM for [Ni^{2+}]. Here, we analyzed the M-DNA complexes without structural deformation at C_s. The band intensities for the bases and the phosphate backbone of the M-DNA complexes are lower relative to the DX DNA crystals without metal ions. The band intensities for A, C, G, T, and PO_4^- decrease in the order of DNA > Zn-DNA > Co-DNA > Cu-DNA > Ni-DNA complexes. Figure 2(f) shows the binding preference for the different metal ions intercalated between the A–T and G–C base pairs and the binding with PO_4^- for the M-DNA complexes. In order to estimate the preference sites for binding, we considered the strongest intensity for each of the A, T, G, C, and PO_4^- Raman bands only. The metal ions were intercalated between the base pairs and were bound with the phosphate backbone sites with binding preferences of 33–34% into A–T base pairs, 34–36% into G–C, and 30–33% into the PO_4^- sites. Zn^{2+} is most preferable toward binding with PO_4^- relative to other metal ions with an order of preference of Zn-DNA > Ni-DNA > Co-DNA > Cu-DNA complexes. These results therefore allow for the quantitative analysis of the metal ion bindings on the specific sites, base pairs, and PO_4^- of the M-DNA complexes.

The conductance of the M-DNA crystals with various metal ion concentrations was measured by using two-terminal measurements with silver electrodes under atmospheric conditions. In this case, each metal ion was added into the DNA buffer solution after the DX crystals were grown on a glass substrate as shown in figure 3(a) in order to maintain deformation-free DX crystals, even slightly above C_s. The schematic diagram of the metal ion-occupied sites, including both substitutional (green solid circles) and interstitial (yellow solid circles) sites in the DNA, are shown in figure 3(b). The AFM images in figures 3(c)–(j) show DNA crystals doped with 4 and 10 mM of [Cu^{2+}]; 1.5 and 8 mM of [Ni^{2+}]; 1, and 8 mM of [Zn^{2+}]; and of 1 and 1.5 mM of [Co^{2+}]. The white dotted lines in the AFM images show the DX crystal boundaries. The insets in the bottom left of figures 3(f) and (j) contain the noise-filtered 2D spectrum images obtained via

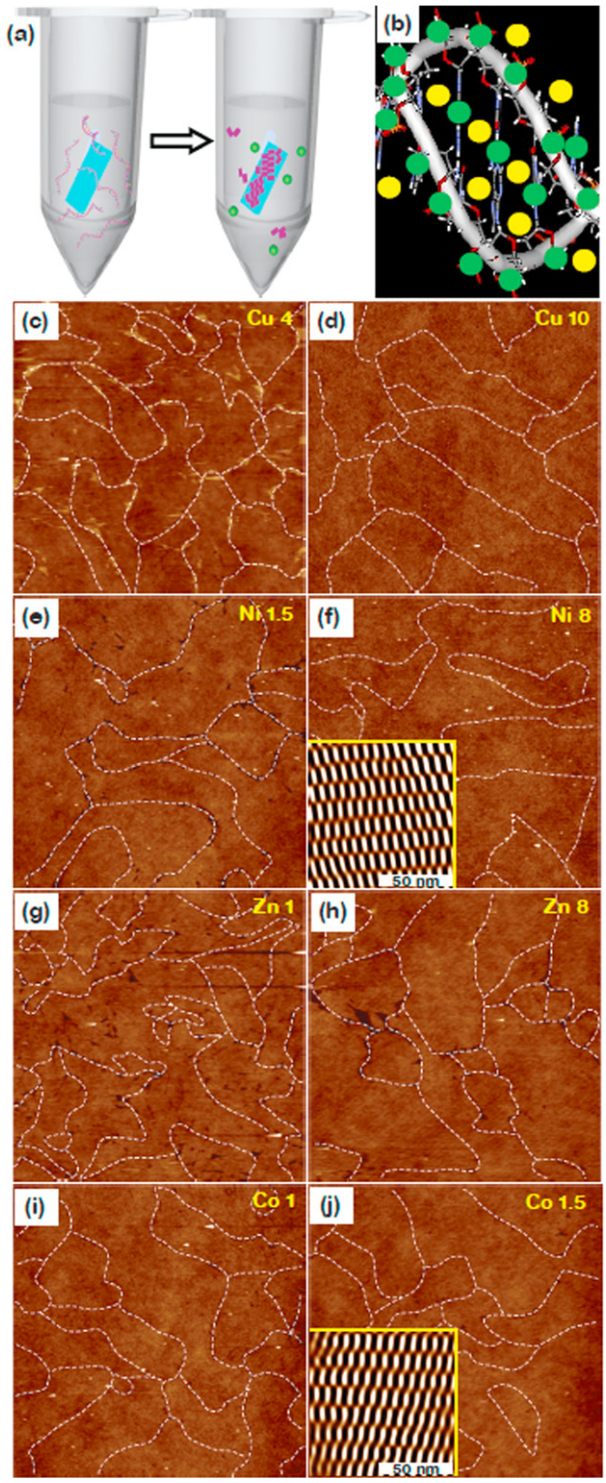

Figure 3. (a) Schematic diagram of metal ions added after annealing. (b) Illustration of the metal ion occupied sites, including both substitutional (green) and interstitial (yellow circle) sites. The AFM images of (c), (d) M-DNA with 4 and 10 mM of $[Cu^{2+}]$ labeled as Cu 4, and Cu 10. (e), (f) M-DNA with 1.5, and 8 mM of $[Ni^{2+}]$. (g), (h) M-DNA with 1 and 8 mM of $[Zn^{2+}]$. (i), (j) M-DNA with 1 and 1.5 mM of $[Co^{2+}]$. The white dotted lines in the AFM images indicate the crystal boundaries. All AFM image scan sizes are of $5 \times 5\ \mu m^2$ unless otherwise stated. The insets in (f) and (g) are the Fourier transform-mode images that show periodicity of the unit DX tiles.

fast Fourier transform and show the periodicities of the unit building blocks. The surface morphologies of the M-DNA crystals constructed by after annealing method, even at higher concentrations, showed them to be similar when compared to the DX crystals without doping.

Figures 4(a)–(d) and (e)–(h) show the *I–V* characteristics and the variation in the resistance according to the different metal ion concentrations at typical voltages. In order to measure the current flow from the M-DNA crystals, we first measured the current passing through a bare glass substrate without DNA crystals and confirmed that no current passed through the electrodes. The resistance of each of the different M-DNA complexes at 3 V was of 1.5, 2.5, 3.1, 3.6, and 7.6 GΩ for the 1.5 mM $[Ni^{2+}]$, 4 mM $[Cu^{2+}]$, 1 mM $[Zn^{2+}]$, 0.6 mM $[Co^{2+}]$, and pristine DNA crystals. In the reverse bias region, the *I–V* curve of all of the M-DNA complexes exhibited a small rectifying behavior whereas a linear curve was observed in the forward bias region. As the voltage was swept from −3 to 3 V, we observed an offset (the current was not zero at 0 V) for all M-DNA complexes, which might be a result of the negative charge of DNA, capacity for charge storage, and/or charge trapped/detrapped nature.

Earlier reports had discussed the electrical properties of single and duplex DNA and M-DNA in a solution or in drop casting [36–38]. In solution, it is difficult to determine whether the conductivity that is measured can be majorly attributed to the DNA molecules or the chemicals in the buffer. In drop casting, there is a problem with respect to the coverage percentage of the DNA between the electrodes. In the present study, we were able to overcome such difficulties by growing the DNA crystals on a given substrate and measuring the *I–V* under dry conditions. Although the DNA crystals had a very thin layer with a thickness of ~0.6 nm in the dry state [38], the M-DNA crystals showed a semiconducting behavior at room temperature, which might be possible due to the hopping of charge carriers through the metal ion-doped DNA crystals.

After doping the metal ions into the DNA crystals, some samples showed an improvement in conductance 2 ~ 5 times higher than that of normal non-doped DNA. A noticeable increase in the current and decrease in the resistance was observed for particular concentration of each metal ion, such as with 4 mM of $[Cu^{2+}]$, 1.5 mM of $[Ni^{2+}]$, 1 mM of $[Zn^{2+}]$, and 0.6 mM of $[Co^{2+}]$. This trend indicates that the C_s of the metal ions into the DNA crystals is the optimum concentration in terms of the conductance. At below C_s, the DNA has more room available for ions to be substituted into the preferred sites, but above C_s, the excess metal ions might coordinate into the DNA molecule at improper interstitial locations.

4. Conclusion

In summary, we fabricated metal ion-modified 2D DNA polycrystalline structures on a glass substrate and studied their crystal stability, structural phase transitions, and *I–V* characteristics by adjusting the concentration of four different

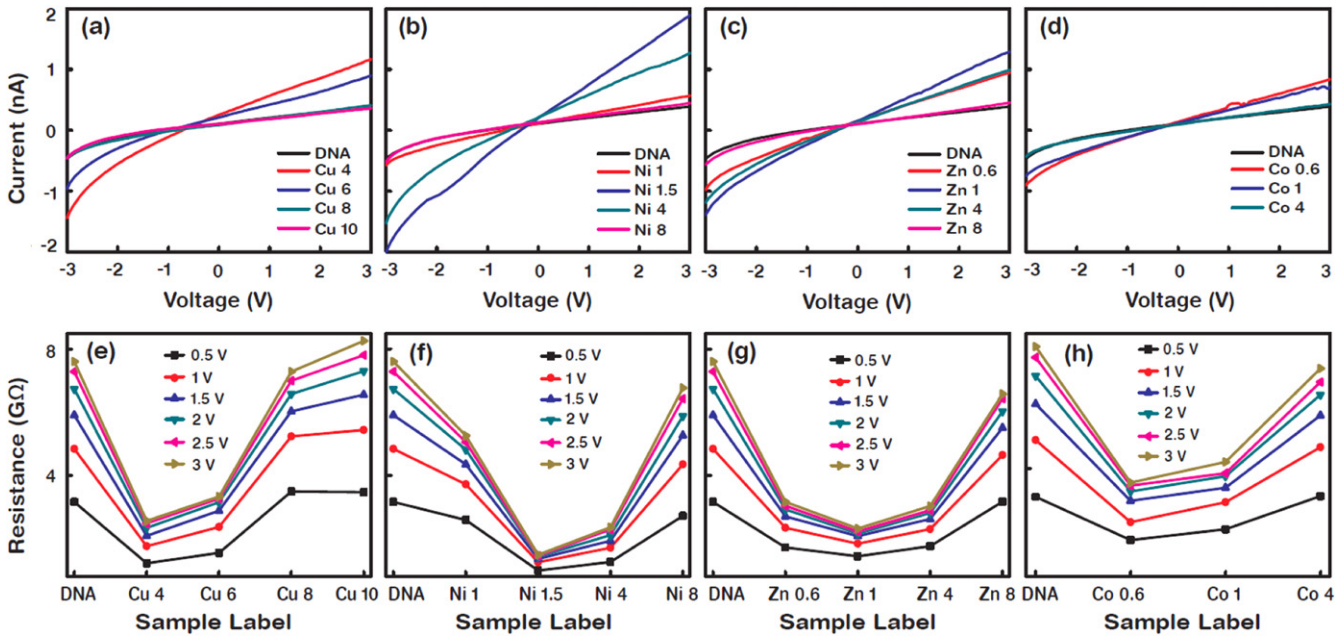

Figure 4. (a)–(d) The variation in the current as a function of voltage at different metal ion concentrations. (e)–(h) The variation in the resistance with various concentrations of metal ions into the DNA crystals—Cu^{2+}-DNA, Ni^{2+}-DNA, Zn^{2+}-DNA, and Co^{2+}-DNA complexes—at typical voltages.

metal ions. The detailed analyses of the Raman spectra of the M-DNA complexes indicate that with an increase in the concentrations of metal ions into DNA, we could observe a considerable decrease on the Raman band intensities throughout the spectrum. Most of the metal ions had a binding preference on the G–C base pairs, A–T base pairs, and PO_4^- sites of DNA, in that order. Interestingly, the increase in the concentration of metal ions up until C_s showed an increase in the current, and a greater concentration showed a decrease in the current. We believe that metal ion doped M-DNA crystals will provide new opportunities to fabricate nano-scale devices and sensors in the near future.

Acknowledgments

This work was supported by the SAIT-SKKU Joint Research Fund 2012 (IO120331-01401-01) to SCP & SHP funded by Samsung Electronics Co. Ltd, by the National Research Foundation of Korea (NRF) (NRF-2013R1A1A2061731 & NRF-2014R1A2A1A11053213) to SRD & SHP, and (NRF-2013R1A2A2A01069023) to GHK funded by the Ministry of Education, Science and Technology (MEST).

References

[1] Rikken G 2011 *Science* **331** 864–5
[2] Bader S D and Parkin S S P 2010 *Annu. Rev. Condens. Matter Phys.* **1** 71–88
[3] Braun E, Eichen Y, Sivan U and Yoseph G B 1998 *Nature* **391** 775–8
[4] Rakitin A *et al* 2001 *Phys. Rev. Lett.* **86** 3670–3
[5] Nam J M, Thaxton C S and Mirkin C A 2003 *Science* **301** 1884–6
[6] Lu Y, Goldsmith B R, Kybert N J and Johnson A T C 2010 *Appl. Phys. Lett.* **97** 083107
[7] Lewis F D 2005 *Photochem. Photobiol.* **81** 65–72
[8] Amin R, Hwang S and Park S H 2011 *Nano* **6** 101–11
[9] Amin R, Kim S, Park S H and LaBean T H 2009 *Nano* **4** 119–39
[10] Seeman N C 2003 *Nature* **421** 427–31
[11] Yin P *et al* 2008 *Science* **321** 824–6
[12] Winfree E, Liu F, Wenzler L A and Seeman N C 1998 *Nature* **394** 539–44
[13] He Y *et al* 2008 *Nature* **452** 198–201
[14] Rothermund P W K 2006 *Nature* **440** 297–302
[15] Steckl A J 2007 *Nat. Photonics* **1** 3–5
[16] Yan H, Park S H, Finkelstein G, Reif J H and LaBean T H 2003 *Science* **301** 1882–4
[17] Sharma J *et al* 2009 *Science* **323** 112–6
[18] Pal S, Deng Z, Ding B, Yan H and Liu Y 2010 *Angew. Chem., Int. Ed. Engl.* **49** 2700–4
[19] Keren K, Berman R S, Bushstab E, Sivan U and Braun E 2003 *Science* **302** 1380–2
[20] Maune H T *et al* 2010 *Nat. Nanotechnology* **5** 61–5
[21] Tanaka K, Tengeiji A, Kato T, Toyama N and Shionoya M 2003 *Science* **299** 1212–3
[22] Dugasani S R *et al* 2014 *ACS Appl. Mater. Interfaces* **6** 17599–17605
[23] Zhang Y, Austin R H, Kraeft J, Cox E C and Ong N P 2002 *Phys. Rev. Lett.* **89** 198102–4
[24] Porath D, Bezryadin A, Vries S D and Dekker C 2000 *Nature* **403** 635–8
[25] Watanabe H, Manabe C, Shigematsu T, Shimotani K and Shimizu M 2001 *Appl. Phys. Lett.* **79** 2462–4
[26] Fink H W and Schonenberger C 1999 *Nature* **398** 407–10
[27] Kasumov A Y *et al* 2001 *Science* **291** 280–2
[28] Moreno-Herrero F *et al* 2003 *Nanotechnology* **14** 128–33

[29] Dugasani S R *et al* 2013 *Sci. Rep.* **3** 1819
[30] Lee J *et al* 2012 *Small* **8** 374–7
[31] Muntean C M, Misselwitz R, Dostal L and Welfle H 2006 *Spectroscopy* **20** 29–35
[32] Otto C, van den Tweel T J J, De Mu F F M and Greve J 1986 *J. Raman Spectrosc.* **17** 289–98
[33] Vasudev M *et al* 2011 *IEEE Trans. Nanotechnology* **10** 35–43
[34] Kulkarni A *et al* 2013 *Sci. Rep.* **3** 2062
[35] Dugasani S R *et al* 2014 *ACS Appl. Mater. Interfaces* **6** 2974–9
[36] Liu H, Li G, Ai H, Li J and Bu Y 2011 *J. Phys. Chem.* C **115** 22547–56
[37] Xu B, Zhang P, Li X and Tao N 2004 *Nano Lett.* **4** 1105–8
[38] Park S H, Prior M W, LaBean T H and Finkelstein G 2006 *Appl. Phys. Lett.* **89** 033901–3